Journal of Computational Applied Mechanics 2022, 53(1): 83-101

DOI: 10.22059/jcamech.2022.334218.669

RESEARCH PAPER

Modified couple stress model for thermoelastic microbeams due to temperature pulse heating

M. A. Kutbi[1] and A. M. Zenkour[1,2*]

[1]*Department of Mathematics, Faculty of Science, King Abdulaziz University, Jeddah 21589, Saudi Arabia*
[2]*Department of Mathematics, Faculty of Science, Kafrelsheikh University, Kafrelsheikh 33516, Egypt*

Abstract

In this research, vibration frequency analysis of a microbeam under a temperature pulse is investigated. In view of the modified couple stress theory and generalized Lord-Shulman (LS) hyperbolic heat conduction model with a single relaxation time, the thermoelastic coupled equations for clamped microbeams have been determined. The analytical terminologies for temperature, deflection, axial displacement, dilatation, flexure moment, couple stress, and axial stress in the microbeam have been acquired utilizing Laplace transform technique. Furthermore, examinations have been displayed in graphs to figure the effect of particular boundaries, for example, the couple stress and pulse of temperature on every one of the thoughts about factors. The couple stress parameter significantly affects all the field distributions. The higher temperature pulses show many disagreements between the results of the present couple stress model and the classical LS one. Alternate estimations of thermal relaxation time have been utilized to the curves anticipated by two unique theories of thermoelasticity that gotten as exceptional instances of the current LS model. Numerical inferences explain that evaluation of deflection anticipated by brand new theory is lower than that of classical LS one.

Keywords: Thermoelasticity; couple stress theory, microbeam; temperature pulse, clamped edges.

Nomenclature

T_0	environment temperature
(x, y, z)	Cartesian coordinates system
u_i	displacement components
σ_{xx}	axial mechanical stress component
$\zeta = E\alpha^2 T_0/\rho c_v$	relaxation strength
e_{ij}	linear strain tensor
t_0	mechanical relaxation time
$\theta = T - T_0$	temperature change
ρ	material density
$\eta = k/\rho c_v$	thermal diffusivity
k	thermal conductivity
ω_i	components of the rotation vector
ϵ_{kij}	alternate tensor
χ_{kl}	symmetric curvature
C_v	specific heat at uniform strain
E	Young's modulus

ν	Poisson's ratio
α	thermal expansion coefficient
δ_{ij}	Kronecker delta function
$\gamma = \alpha E/(1-2\nu)$	coupling parameter
$\mu = E/2(1+\nu)$	shear modulus
L	length of the microbeam
ℓ_0	couple stress (material length scale) coefficient.
b	width of the microbeam
h	the thickness of the microbeam
u, w	Axial displacement and transverse deflection
$A = bh$	beam cross-section area
$I = bh^3/12$	inertia moment of a cross-section
EI	flexural rigidity of microbeam
M_T	thermal moment

1. Introduction

Micro-size mechanical resonators have high affectability and quick reactions and are broadly utilized as sensors and antennae. Miniaturized scale and nano-mechanical resonant circuits have pulled in great thought actually because of their various basic innovative applications.

Precise investigation of numerous impacts on the attributes of resonators, for example, resounding frequencies and quality effects, is essential for inventing high-implementation mechanisms. Several investigators have concentrated on the vibration and temperature exchange technique of beams [1-6]. Progressed devices that have arisen on the establishment of advanced science, the resonators, microscale switches, phones, mirrors, and siphons are instances of this methodology [7, 8].

The traditional elasticity theory is not prepared for getting the size impact of micro shape and is reasonable to contemplate material lead on the macro-scale. The clarification behind such deviation is seen to be the significant impact of microstructure [9, 10]. Therefore, the non-classical models, for example, the gradient of strain or couple stress are used to consider lead of structures in such scales.

In recent years, several theories of a size-dependent structure such as couple stress theory (CST) [11], modified couple stress theory (MCST) [12-14], strain gradient elasticity theory (SGET) [15, 16], higher and lower-order nonlocal strain gradient theories (NSGT) [17-19] nonlocal elasticity theory (NET) [20-24] are introduced. These theories consist of evidence about the interfacial forces and internal lengths that are presented as small-scale influences on the nonlocal theory of elasticity [25-27]. In Rajneesh [28], the response of a thermoelastic beam is discussed by utilizing the theory of modified couple stress (MCS) exposed to the thermal resource. Park and Gao [29] studied a thin beam based on Euler–Bernoulli's theory using the MCS theory. In view of the generalized thermoelasticity and MCS theories, many articles have been established [30-33]. Shishesaz et al. [34] presented the thermoelastic behavior of (functionally graded) FG nanodisks based on strain gradient theory. Hadi et al. [35] investigated the free vibration of three-directional FG Euler–Bernoulli nanobeam with small-scale effects. Hadi et al. [36] used the couple-stress theory to capture size effects in Euler-Bernoulli FG nanobeams. Hosseini et al. [37] presented the mechanical behavior of different nanostructures by using non-classical elasticity theories. Khoram et al. [38] presented the bending of bidirectional FG nanobeams under mechanical loads and magnetic force.

The dynamic propagation of heat disturbances in solids in engineering and physics is of fantastic practical importance. For the classical theory of heat conduction including the Fourier equation, there are many pathological anomalies, particularly for cases with very short transients or very low temperatures near absolute zero. In comparison, modified non-Fourier thermal conduction theories based on the general concept of heatstroke relaxation have been proposed in the classical theory to explain the finite rates of heatwave propagation and propagation of thermally induced stress waves in contrast to the classical thermoelastic theories where the distortions are in temperature. It is meant to spread at unlimited speeds. Therefore, some non-Fourier temperature control methods have been proposed and have been the focus of active research for recent decades. This so-called classical paradox is free of generalized thermoelasticity theory.

Lord and Shulman (LS) [39], introduced a generalized thermoelasticity model by modifying the governing equations of classical coupled theory with the inclusion of a time of relaxation. Therefore, the law of heat conduction is restored by the concept of heat conduction proposed by Cattaneo-Vernotte. The problem of the infinite distribution

of thermal signals is solved by this theory. The LS model exhibited the generalized thermoelasticity theory with single relaxation time, in which a changed law.

In this effort, the modified couple stress (MCS) theory, generalized theory of thermoelasticity (LS) as well as the linear Euler–Bernoulli beam (EBB) theory are combined and an associated mathematical model is constructed. The introduced model is employed to study the thermoelastic interaction of microbeam resonators exposed to a temperature pulse. Unlike many problems that use the harmonic solution, the model was solved using the Laplace transform procedure. A numerical method is utilized to get the inverse Laplace transform of deflection and temperature behavior of microbeam in the physical domain. The impacts of the different parameters such as temperature pulse, relaxation time, and material length-scale on responses of physical fields of microbeam are analyzed. The expressions for the physical variables have been graphically processed for a microbeam of Nickel.

2. Governing equations

The Fourier's law that connects heat flux vector $\boldsymbol{q}$ to temperature gradient $\nabla\theta$ is given here

$$\boldsymbol{q}(\boldsymbol{x},t) = -k\nabla\theta(\boldsymbol{x},t), \tag{1}$$

in which k implies the thermal conductivity coefficient, $\theta = T - T_0$, and T_0 represents the environmental temperature. The energy equation is given by

$$\rho c_v \frac{\partial\theta}{\partial t} + \gamma T_0 \frac{\partial}{\partial t}(\operatorname{div}\boldsymbol{u}) = -\nabla\cdot\boldsymbol{q} + Q, \tag{2}$$

where Q implies the heat source, c_v denotes the specific heat, ρ represents the density, $\boldsymbol{u}$ represents displacement vector and $\operatorname{div}\boldsymbol{u} = e = e_{kk}$ denotes volumetric strain and e_{ij} represents strain tensor. Fourier law has been replaced by the Cattaneo-Vernotte model of thermal conductivity that includes, both heat flow and its time derivatives and a relaxation time τ_0 and given by

$$\left(1 + \tau_0 \frac{\partial}{\partial t}\right)\boldsymbol{q} = -K\nabla\theta. \tag{3}$$

In sequence with the energy conservative law (2) with Eq. (3), we obtain the modified heat conduction equation with phase lags as

$$\left(1 + \tau_0 \frac{\partial}{\partial t}\right)\left(\rho c_v \frac{\partial\theta}{\partial t} + \gamma T_0 \frac{\partial e}{\partial t} - Q\right) = k\nabla^2\theta. \tag{4}$$

The constitutive relations

$$e_{ij} = \frac{1+\nu}{E}\sigma_{ij} + \left(\alpha\theta - \frac{\nu}{E}\sigma_{kk}\right)\delta_{ij}. \tag{5}$$

The constitutive equation of couple stress tensor m_{ij} will be in the form [12, 40]:

$$m_{ij} = 2\mu\ell_0^2\chi_{ij}. \tag{6}$$

The symmetric curvature tensor χ_{kl} in terms of rotation gradient can be created as:

$$\chi_{kl} = \frac{1}{2}\left(\frac{\partial\omega_k}{\partial x_l} + \frac{\partial\omega_l}{\partial x_k}\right). \tag{7}$$

The rotation vector ω_i is associated with the infinitesimal displacement vector as follows:

$$\omega_i = \frac{1}{2}\epsilon_{ijk}u_{k,j}. \tag{8}$$

The small strain-displacement relations are

$$e_{kl} = \frac{1}{2}\left(\frac{\partial u_k}{\partial x_l} + \frac{\partial u_l}{\partial x_k}\right). \tag{9}$$

3. Mathematical model

The rectangular system of coordinates (x, y, z) is introduced to investigate a thermoelastic microbeam. We consider that at the left end of the microbeam, the origin of the coordinates is fixed. The microbeam of length $L(0 \le x \le L)$,

width $b(-b/2 \le y \le +b/2)$, and constant thickness $h(-h/2 \le z \le +h/2)$ as shown in Figure 1. The displacements in x, y, and z directions due to Bernoulli-Euler beam theory are provided by [3]:

$$u = -z\frac{\partial w}{\partial x}, \quad v = 0, \quad w = w(x,t), \tag{10}$$

where u and w represent the longitudinal and transverse displacements. The replacement of Eq. (10) into Eq. (8), provides the components of the rotation vector as

$$\omega_y = -\frac{\partial w}{\partial x}, \quad \omega_x = \omega_z = 0. \tag{11}$$

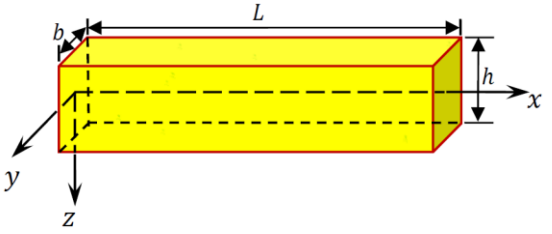

Fig. 1: The schematic diagram for the microbeam.

Presenting Eq. (11) into Eq. (7), the nonvanishing curvature χ_{ij} and deviatoric parts of the couple stress components are given by:

$$\chi_{xy} = -\frac{1}{2}\frac{\partial^2 w}{\partial x^2}, \tag{12}$$

$$m_{xy} = -\mu\ell_0^2\frac{\partial^2 w}{\partial x^2}. \tag{13}$$

Equations (1) considered the plane stress conditions and has nonzero elements along x-axis. With aid of Eq. (10), the nonzero strain and the axial stress are expressed as

$$e_{xx} = -z\frac{\partial^2 w}{\partial x^2}, \quad e_{yy} = e_{zz} = \nu z\frac{\partial^2 w}{\partial x^2} + \alpha(1+\nu)\theta, \tag{14}$$

$$\sigma_{xx} = -E\left(z\frac{\partial^2 w}{\partial x^2} + \alpha\theta\right). \tag{15}$$

In addition, the cubical dilatation will be

$$e = e_{kk} = -(1-2\nu)z\frac{\partial^2 w}{\partial x^2} + 2\alpha(1+\nu)\theta, \tag{16}$$

The bending moment resultant M of the microbeam can be considered by the practice of the formula [28]:

$$M = b\int_{-\frac{h}{2}}^{\frac{h}{2}}\left(m_{xy} + z\sigma_x\right)\mathrm{d}z. \tag{17}$$

By using Eqs. (6), (13), and (14) into Eq. (15), the flexure moment of the cross-section may be expressed as

$$M(x,t) = -EI\left(\frac{\partial^2 w}{\partial x^2} + \alpha M_T\right) - \mu\ell_0^2 A\frac{\partial^2 w}{\partial x^2}, \tag{18}$$

where the thermal moment M_T is given by

$$M_T = \frac{12}{h^3}\int_{-h/2}^{h/2}\theta(x,z,t)z\ \mathrm{d}z. \tag{19}$$

Based on total strain energy, the dynamic equation of microbeam can be expressed as

$$\frac{\partial^2 M}{\partial x^2} = \rho A\frac{\partial^2 w}{\partial t^2}. \tag{20}$$

The use of Eq. (18) into Eq. (20) yields the dynamic equation of beam in the form

$$(EI + \mu\ell_0^2 A)\frac{\partial^2 w}{\partial x^4} + \rho A\frac{\partial^2 w}{\partial t^2} + \alpha EI\frac{\partial^2 M_T}{\partial x^2} = 0. \tag{21}$$

Introducing Eq. (16) into Eq. (4) and omitting the force Q, the heat conduction equation may be composed as:

$$\eta\left(\frac{\partial^2\theta}{\partial x^2}+\frac{\partial^2\theta}{\partial z^2}\right)=\left(1+\tau_0\frac{\partial}{\partial t}\right)\left[(1+\xi)\frac{\partial\theta}{\partial t}-\frac{\zeta}{\alpha}\left(z\frac{\partial^3 w}{\partial t\partial x^2}\right)\right], \tag{22}$$

where

$$\xi=\frac{2(1+\nu)\zeta}{(1-2\nu)},\quad \zeta=\frac{\alpha^2 E T_0}{\rho c_\nu}. \tag{23}$$

For the present microbeam, expecting that temperature is a sinusoidal variety along with the thickness, i.e.,

$$\theta(x,z,t)=\Theta(x,t)\sin\left(\frac{\pi z}{h}\right). \tag{24}$$

The use of Eq. (24) into Eqs. (17) and (21) after some numerical activities provide

$$M(x,t)=-(EI+\mu\ell_0^2 A)\frac{\partial^2 w}{\partial x^2}-EI\frac{24\alpha}{\pi^2 h}\Theta, \tag{25}$$

$$(EI+\mu\ell_0^2 A)\frac{\partial^2 w}{\partial x^4}+\rho A\frac{\partial^2 w}{\partial t^2}+EI\frac{24\alpha}{\pi^2 h}\frac{\partial^2\Theta}{\partial x^2}=0. \tag{26}$$

Integrating Eq. (22) concerning z after multiplying by z through microbeam thickness from $-h/2$ to $h/2$ and taking into consideration Eq. (24), gives

$$\eta\left(\frac{\partial^2\Theta}{\partial x^2}-\frac{\pi^2}{h^2}\Theta\right)=\left(1+\tau_0\frac{\partial}{\partial t}\right)\left[(1+\xi)\frac{\partial\Theta}{\partial t}-\frac{\zeta\pi^2 h}{24\alpha}\frac{\partial}{\partial t}\left(\frac{\partial^2 w}{\partial x^2}\right)\right]. \tag{27}$$

For effortlessness we will utilize the accompanying non-dimensional amounts:

$$(x',u')=\frac{1}{L}(x,u),\quad (z',w')=\frac{1}{h}(z,w),\quad \Theta'=\alpha\Theta,\quad (t',t_0')=\frac{c}{L}(t,t_0),$$
$$m_{xy}'=\frac{h}{E}m_{xy},\quad \sigma_x'=\frac{\sigma_x}{E},\quad M'=\frac{M}{bEh^2},\quad c=\sqrt{\frac{E}{\rho}}. \tag{28}$$

Applying non-dimensional variables appeared in Eq. (28), the fundamental equations may be altered as follows (dropping the primes for convenience)

$$a_1\frac{\partial^4 w}{\partial x^4}+\frac{\partial^2 w}{\partial t^2}+a_2\frac{\partial^2\Theta}{\partial x^2}=0, \tag{29}$$

$$\frac{\partial^2\Theta}{\partial x^2}-a_3\Theta=\left(1+\tau_0\frac{\partial}{\partial t}\right)\left[a_4\frac{\partial\Theta}{\partial t}-a_5\frac{\partial}{\partial t}\left(\frac{\partial^2 w}{\partial x^2}\right)\right], \tag{30}$$

$$\sigma_x=-z\frac{h^2}{L^2}\frac{\partial^2 w}{\partial x^2}-\Theta\sin(\pi z), \tag{31}$$

$$m_{xy}=-\frac{h^2\mu\ell_0^2}{L^2 E}\frac{\partial^2 w}{\partial x^2}, \tag{32}$$

$$M(x,t)=-a_1\frac{\partial^2 w}{\partial x^2}-a_2\Theta, \tag{33}$$

$$u=-z\frac{h^2}{L^2}\frac{\partial w}{\partial x}, \tag{34}$$

$$e=-(1-2\nu)z\frac{h^2}{L^2}\frac{\partial^2 w}{\partial x^2}+2\alpha(1+\nu)\Theta\sin(\pi z), \tag{35}$$

where

$$a_1=\left(\frac{\ell_0^2\mu}{L^2E}+\frac{h^2}{12L^2}\right),\quad a_2=\frac{2}{\pi^2},\quad a_3=\frac{\pi^2L^2}{h^2},\quad a_4=(1+\xi)\frac{cL}{\eta},\quad a_5=\frac{\pi^2h^2c\zeta}{24L\eta}. \tag{36}$$

Now, we will present the initial and boundary conditions of the problem. The initial conditions of the considered issue are thought to be homogeneous as

$$w(x,t)|_{t=0}=\left.\frac{\partial w(x,t)}{\partial t}\right|_{t=0}=0,\quad \Theta(x,t)|_{t=0}=\left.\frac{\partial\Theta(x,t)}{\partial t}\right|_{t=0}=0. \tag{37}$$

To take care of the problem, the accompanying boundary conditions are considered. Firstly, let the instance of the two edges of the microbeam be clamped, for example

$$w(x,t)|_{x=0,L} = 0, \quad \frac{\partial w(x,t)}{\partial x}\Big|_{x=0,L} = 0. \tag{38}$$

Second, we assume that the plane $x = 0$ of microbeam is subjected to temperature pulse as

$$\Theta(0,t) = \Theta_0 \begin{cases} \sin(\omega t), & 0 \le t \le \frac{\pi}{\omega}, \\ 0, & t > \frac{\pi}{\omega}, \end{cases} \tag{39}$$

where Θ_0 is the amplitude and ω is the temperature pulse. Also, the temperature at end boundary $x = L$ ought to fulfill the accompanying connection

$$\frac{\partial \Theta}{\partial x} = 0, \quad x = L. \tag{40}$$

4. Laplace transform domain and its inversion

Taking the Laplace transform characterized by the connection

$$\bar{f}(x,s) = \int_0^\infty \mathrm{e}^{-st} f(x,t)\mathrm{d}t, \tag{41}$$

to the two sides of Eqs. (29)-(35) and utilizing homogeneous initial conditions in Eq. (37), we obtain field equations in Laplace change space as

$$a_1 \frac{\mathrm{d}^4 \bar{w}}{\mathrm{d}x^4} + s^2 \bar{w} + a_2 \frac{\mathrm{d}^2 \bar{\theta}}{\mathrm{d}x^2} = 0, \tag{42}$$

$$\left(\frac{\mathrm{d}^2}{\mathrm{d}x^2} - a_6\right)\bar{\theta} = -a_7 \frac{\mathrm{d}^2 \bar{w}}{\mathrm{d}x^2}, \tag{43}$$

$$\bar{\sigma}_x = -z\frac{h^2}{L^2}\frac{\mathrm{d}^2 \bar{w}}{\mathrm{d}x^2} - \bar{\theta}\sin(\pi z), \tag{44}$$

$$\bar{m}_{xy} = -\frac{h^2 \mu \ell_0^2}{L^2 E}\frac{\mathrm{d}^2 \bar{w}}{\mathrm{d}x^2}, \tag{45}$$

$$\bar{M} = -a_1 \frac{\mathrm{d}^2 \bar{w}}{\mathrm{d}x^2} - a_2 \bar{\theta}, \tag{46}$$

$$\bar{u} = -z\frac{h^2}{L^2}\frac{\mathrm{d}\bar{w}}{\mathrm{d}x}, \tag{47}$$

$$\bar{e} = -(1-2\nu)z\frac{h^2}{L^2}\frac{\mathrm{d}^2 \bar{w}}{\mathrm{d}x^2} + 2\alpha(1+\nu)\bar{\theta}\sin(\pi z). \tag{48}$$

It is noted that the over bar image means its Laplace transform, s indicates Laplace parameter and

$$a_6 = a_3 + s(1+\tau_0 s)a_4, \quad a_7 = s(1+\tau_0 s)a_5. \tag{49}$$

Elimination $\bar{\theta}$ or $\bar{w}$ from Eqs. (42) and (43) provides the following differential equation for $\bar{w}$ or $\bar{\theta}$:

$$\left(\frac{\mathrm{d}^6}{\mathrm{d}x^6} - b_2\frac{\mathrm{d}^4}{\mathrm{d}x^4} + b_1\frac{\mathrm{d}^2}{\mathrm{d}x^2} - b_0\right)\{\bar{w}, \bar{\theta}\} = 0, \tag{50}$$

where the coefficients b_i are given by

$$b_2 = a_6 + \frac{a_2 a_7}{a_1}, \quad b_1 = \frac{s^2}{a_1}, \quad b_0 = \frac{a_6 s^2}{a_1}. \tag{51}$$

Introducing m_i $(i = 1,2,3)$, Eq. (48) can be given by

$$(D^2 - m_1^2)(D^2 - m_2^2)(D^2 - m_3^2)\{\bar{w}, \bar{\Theta}\} = 0, \tag{52}$$

where $D = \mathrm{d}/\mathrm{d}x$ and m_1^2, m_2^2 and m_3^2 are characteristic roots of

$$m^6 - b_2 m^4 + b_1 m^2 + b_0 = 0. \tag{53}$$

The roots of Eq. (51) satisfy the well-known relations:

$$m_1^2 + m_2^2 + m_2^2 = b_2, \quad m_1^2 m_2^2 + m_2^2 m_3^2 + m_3^2 m_1^2 = b_1, \quad m_1^2 m_2^2 m_2^2 = b_0. \tag{54}$$

The solution of Eqs. (50) in Laplace domain may be expressed as

$$\bar{w} = \sum_{i=1}^{3}[A_i \cosh(m_i x) + B_i \sinh(m_i x)], \tag{55}$$

$$\bar{\theta} = \sum_{i=1}^{3} \beta_i [A_i \cosh(m_i x) + B_i \sinh(m_i x)], \tag{56}$$

where A_i and B_i are constant coefficients differing on s and

$$\beta_i = \frac{a_7 m_i^2}{a_6 - m_i^2}. \tag{57}$$

The flexural moment M appeared in Eq. (46) in the Laplace domain with the help of Eqs. (55) and (56) is given by

$$\bar{M} = -\sum_{i=1}^{3} \gamma_i [A_i \cosh(m_i x) + B_i \sinh(m_i x)], \tag{58}$$

where

$$\gamma_i = a_1 m_i^2 + a_2 \beta_i. \tag{59}$$

Additionally, the axial displacement in the Laplace domain of utilizing Eq. (47) takes the form

$$\bar{u} = -z \frac{h^2}{L^2} \sum_{i=1}^{3} m_i [A_i \sinh(m_i x) + B_i \cosh(m_i x)]. \tag{60}$$

Besides, the dilatation is given by

$$\bar{e} = \sum_{i=1}^{3} \bar{\gamma}_i [A_i \cosh(m_i x) + B_i \sinh(m_i x)], \tag{61}$$

where

$$\bar{\gamma}_i = -(1 - 2\nu) z \frac{h^2}{L^2} m_i^2 + 2\alpha(1 + \nu) \sin(\pi z)\, \beta_i. \tag{62}$$

Additionally, the axial stress and couple stress according to Eqs. (44) and (45) become

$$\bar{\sigma}_x = -\sum_{i=1}^{3} \hat{\gamma}_i [A_i \cosh(m_i x) + B_i \sinh(m_i x)], \tag{63}$$

$$\bar{m}_{xy} = -\sum_{i=1}^{3} \check{\gamma}_i [A_i \cosh(m_i x) + B_i \sinh(m_i x)], \tag{64}$$

where

$$\hat{\gamma}_i = m_i^2 z \frac{h^2}{L^2} + \beta_i \sin(\pi z), \quad \check{\gamma}_i = \frac{h^2 \mu \ell_0^2}{L^2 E} m_i^2. \tag{65}$$

In the Laplace transform domain, boundary conditions (37)-(40) are given by

$$\bar{w}(x,s)|_{x=0,1} = 0, \quad \left.\frac{\mathrm{d}\bar{w}(x,s)}{\mathrm{d}x}\right|_{x=0,1} = 0, \tag{66}$$

$$\bar{\theta}(x,s)|_{x=0} = \frac{\omega \theta_0}{s^2 + \omega^2} = \bar{G}(s), \tag{67}$$

$$\frac{\partial \bar{\theta}}{\partial x} = 0, \quad x = 1. \tag{68}$$

The solution of the exceeding arrangement of direct conditions provides the obscure parameters A_i and B_i. This finishes the solution to the problem in the Laplace domain.

To achieve numerical results in the physical domain, we employ the Riemann-sum approximation technique. In this strategy, any function $\bar{f}(x,z,s)$ in space of Laplace transform is upset to physical domain $f(x,z,t)$ by applying the notable equation [41]

$$f(x,z,t) = \frac{\mathrm{e}^{\varrho t}}{t}\left[\frac{1}{2}\mathrm{Re}\{\bar{f}(x,z,\varrho)\} + \mathrm{Re}\left\{\sum_{n=0}^{N}\left(\bar{f}\left(x,z,\varrho + \frac{\mathrm{i}n\pi}{t}\right)(-1)^n\right)\right\}\right], \tag{69}$$

where Re is the real part of a function, $\mathrm{i} = \sqrt{-1}$ and $\varrho \approx 4.7/t$ [42].

5. Numerical results

The numerical examination of the systematic outcomes got in the past parts concerning deflection, thermodynamic temperature change, axial displacement, flexural moment, and stress in the beam will be discussed here. The effect of

temperature pulse, the lack and existence of couple stress, and thermal relaxation time on field variables are investigated. It is expected that the properties of the beam are assumed as:

$$E = 56\ \text{GPa},\quad k = 429\ (\text{W/mK}),\quad \rho = 10500\ (\text{kg/m}^3),\quad C_v = 234\ (\text{J/K kg}),$$
$$\alpha = 2.0 \times 10^{-5}\ (1/\text{K}),\quad T_0 = 293\ \text{K},\quad \nu = 0.36. \tag{70}$$

The aspect ratio of microbeam is fixed as $L/h = 10$, the thickness is assumed as $h = 0.1$ μm and the dimensionless time is fixed as $t = 0.3$. Also, the dimensionless couple stress parameter is fixed as $\ell = \ell_0/L$. Other parameters are assumed (except otherwise stated) as $\ell = 0.2$, $\omega = 0.2$, $\tau_0 = 0.01$, and $z = h/3$. The values of temperature change θ, distributions of deflection w, distributions of axial displacement u, dilatation e, thermal moment M, couple stress m_{xy}, and axial stress σ_x are defined according to Eq. (69). Numerical outcomes have been carried out. The numerical outcomes have been exhibited in detail in Figs. 2-8.

5.1. *Couple stress effect*

The impact of couple stress on numerical calculations of field quantities is illustrated in Figs. 2-8 in the presence ($\ell \neq 0$) and absence of couple stress coefficient ($\ell = 0$). The present couple stress model expects higher values of all field quantities as compared with that of simple FS theory.

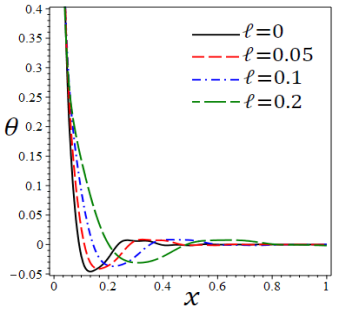

Fig. 2: Effect of modified couple stress coefficient ℓ on the temperature θ of simple LS theory ($\tau_0 = 0.01$) versus axial direction.

Figure 2 demonstrates the temperature change θ of the microbeam through the x-axis for $\ell = 0$, 0.05, 0.1, and 0.2 when the parameters ω and τ_0 are fixed. It can be concluded that the value of ℓ has a sensitive effect on the temperature values. Also, the temperature decreases monotonically in microbeams in direction of wave propagation. The wavelength of the temperature wave increases as ℓ increases. The smallest wavelength occurs when $\ell = 0$.

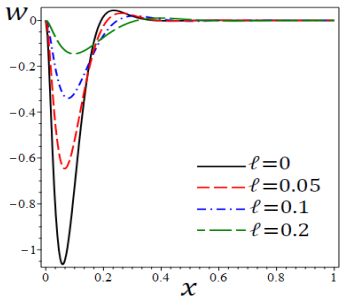

Fig. 3: Effect of modified couple stress coefficient ℓ on the deflection w of simple LS theory ($\tau_0 = 0.01$) versus axial direction.

Figure 3 displays the variations of deflection w of the microbeam for the distinct four values of material length scale ℓ. As shown in this figure, compared to the simple LS theory ($\ell = 0$) that considers the impact of a material length parameter along with the impact of deflection on MCS LS theory, leads to a decrease in lateral deflection of microbeam. Therefore, given the parameter of the material length scale, the minimum, and maximum deflection decrease. It is noticed that the deflection dropped from zero to its minimum value at $x = 0.058$, then it raises to its maximum value at $x = 0.236$, then it decreases gradually as x increased and vanishes again when $x = 0$. The amplitude of the deflection wave increases as ℓ decreases.

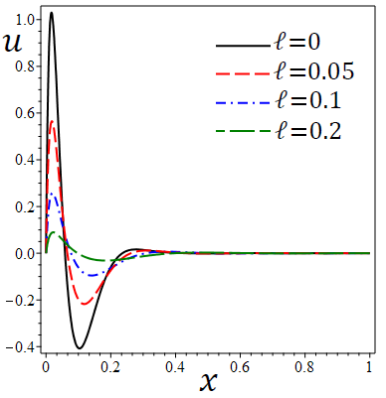

Fig. 4: Effect of modified couple stress coefficient ℓ on the axial displacement u of simple LS theory ($\tau_0 = 0.01$) versus axial direction.

Figure 4 presents the distribution of axial displacement u of microbeam for distinct values of parameter ℓ. It tends to be seen that parameter ℓ greatly affects the distribution of displacement u. The amplitude of the displacement wave is fading away with the increase in x-axis. The wavelength of the displacement wave may be constant for different coefficients ℓ while the maximum amplitude occurs when $\ell = 0$.

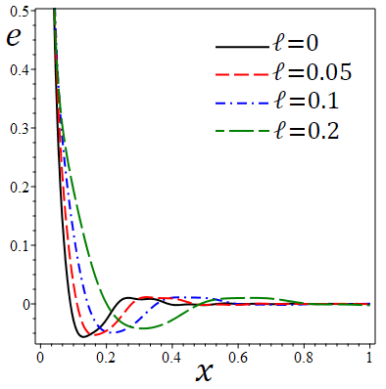

Fig. 5: Effect of modified couple stress coefficient ℓ on the dilatation e of simple LS theory ($\tau_0 = 0.01$) versus axial direction.

Figure 5 presents the distribution of dilatation e of microbeam for distinct values of parameter ℓ. Once again, the parameter ℓ greatly affects the distribution of dilatation e. The amplitude of the dilatation wave is fading away with the increase in x-axis. The wavelength of the displacement wave is rapidly increasing as ℓ increases while the amplitude is slowly decreasing as ℓ decreases.

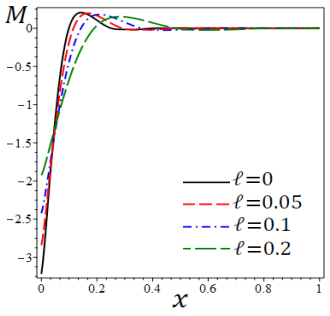

Fig. 6: Effect of modified couple stress coefficient ℓ on the moment M of simple LS theory ($\tau_0 = 0.01$) versus axial direction.

Figure 6 illustrates the variety of bending moment M through axial distance x in the presence and absence of couple stress in the microbeam. It is noticed that the couple stress coefficient ℓ is significantly affected the bending moment distribution.

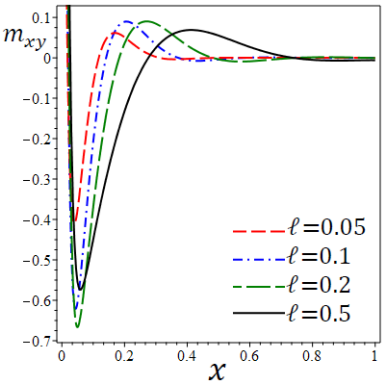

Fig. 7: Effect of modified couple stress coefficient ℓ on the couple stress m_{xy} of simple LS theory ($\tau_0 = 0.01$) versus axial direction.

Figure 7 presents the distribution of couple stress m_{xy} of microbeam for distinct values of parameter $\ell > 0$. It tends to be seen that parameter ℓ greatly affects the distribution of m_{xy}. The amplitude of the couple stress wave is fading away with the increase in x-axis. It is clear that the wavelength is increasing with the increase in ℓ. The maximum amplitude value occurs when $\ell = 0.2$.

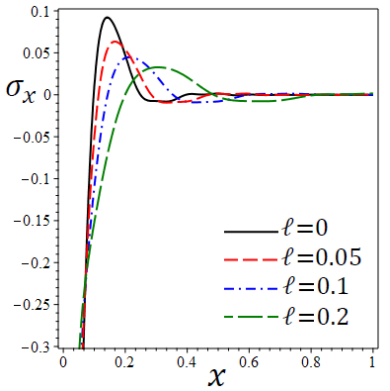

Fig. 8: Effect of modified couple stress coefficient ℓ on the axial stress σ_x of simple LS theory ($\tau_0 = 0.01$) versus axial direction.

Figure 8 presents the distribution of axial stress σ_x of microbeam for distinct values of parameter ℓ. It tends to be seen that parameter ℓ greatly affects the distribution of σ_x. The amplitude of the stress wave is fading away with the increase in x-axis. For the stress wave, the wavelength is increasing with the increase in ℓ while the amplitude is increasing with the decrease in ℓ. The maximum amplitude value occurs when $\ell = 0$.

5.2. *The impact of temperature pulse*

The effects of the temperature pulse ω on all fields are displayed in Figs. 9-15. It is assumed that the thermal relaxation time $\tau_0 = 0.01$ and the modified couple stress coefficient $\ell = 0.2$. Figure 9 demonstrates the temperature change θ of the microbeam through the x-axis for different values of ω when the parameters ℓ and τ_0 are fixed. It can be concluded that the value of the temperature pulse ω has a sensitive effect on the temperature values. Also, the temperature decreases monotonically in microbeams in direction of wave propagation. The amplitude of the temperature wave increases as ω increases.

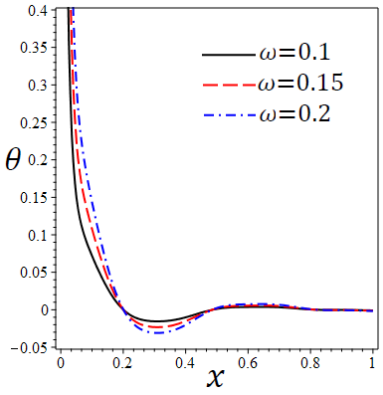

Fig. 9: Effect of temperature pulse ω on the temperature θ of coupled stress LS theory ($\ell = 0.2$, $\tau_0 = 0.01$) versus axial direction.

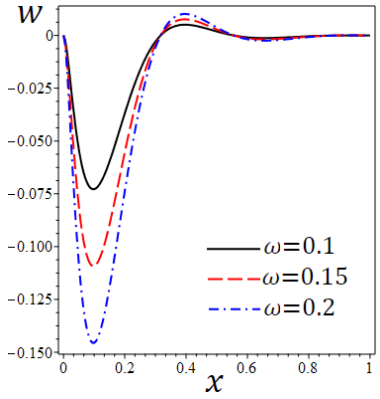

Fig. 10: Effect of temperature pulse ω on the deflection w due to coupled stress LS theory ($\ell = 0.2$, $\tau_0 = 0.01$) versus axial direction.

Figure 10 displays the variations of deflection w of the microbeam for distinct values of temperature pulse ω. It is noticed that the deflection waves have the same wavelength while the amplitude of the deflection wave increases as ω increases.

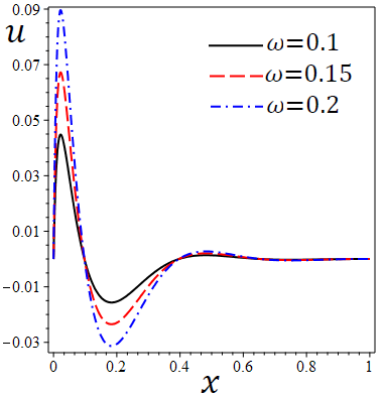

Fig. 11: Effect of temperature pulse ω on the axial displacement u due to coupled stress LS theory ($\ell = 0.2$, $\tau_0 = 0.01$) versus axial direction.

Figure 11 presents the distribution of axial displacement u of microbeam for the distinct values of temperature pulse ω. The parameter ω greatly affects the distribution of displacement u. The amplitude of the displacement wave is fading away with the increase in x-axis. The wavelength of the displacement wave is constant while the maximum amplitude occurs when $\omega = 0.2$.

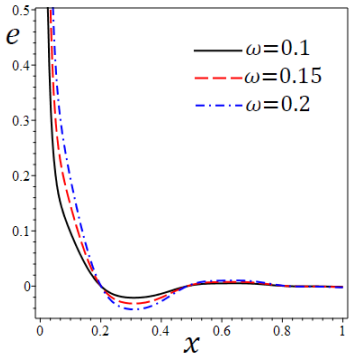

Fig. 12: Effect of temperature pulse ω on the dilatation e due to classical LS theory ($\tau_0 = 0.01$) versus axial direction.

Figure 12 presents the distribution of dilatation e of microbeam for distinct values of temperature pulse ω. The parameter ω greatly affects the distribution of dilatation e. The amplitude of the dilatation wave is fading away with the increase in x-axis. The wavelength of the displacement wave is constant while the amplitude is decreasing as ω decreases.

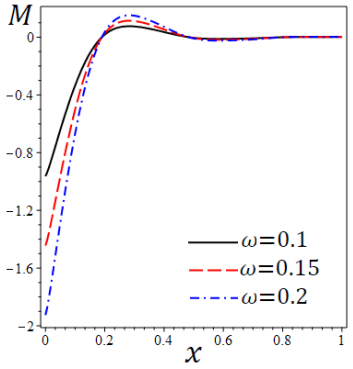

Fig. 13: Effect of temperature pulse ω on the moment M due to coupled stress LS theory ($\ell = 0.2$, $\tau_0 = 0.01$) versus axial direction.

Figure 13 illustrates the variety of bending moment M through axial distance x for distinct values of temperature pulse ω. It is noticed that the temperature pulse parameter ω is significantly affected the bending moment distribution. The moment M is no longer increasing as x increases and has its maximum value when $\omega = 0.2$.

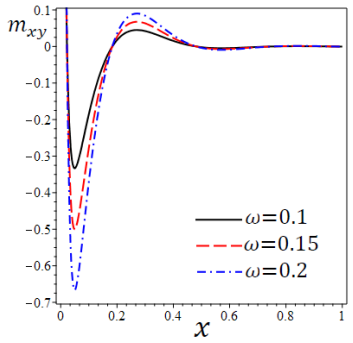

Fig. 14: Effect of temperature pulse ω on the couple stress m_{xy} of coupled stress LS theory ($\ell = 0.2$, $\tau_0 = 0.01$) versus axial direction.

Figure 14 presents the distribution of couple stress m_{xy} of microbeam for the distinct values of temperature pulse ω. It tends to be seen that parameter ω greatly affects the distribution of m_{xy}. The amplitude of the couple stress wave

is fading away with the increase in x-axis. The wavelength of the stress wave is constant while the amplitude is increasing with the increase in ω.

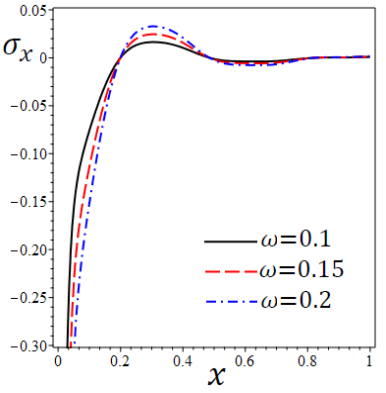

Fig. 15: Effect of temperature pulse ω on the axial stress σ_x due to coupled stress LS theory ($\ell = 0.2$, $\tau_0 = 0.01$) versus axial direction.

Figure 15 presents the distribution of axial stress σ_x of microbeam for the distinct values of temperature pulse ω. The parameter ω greatly affects the distribution of σ_x. The amplitude of the stress wave is fading away with the increase in x-axis. The wavelength of the stress wave is constant while the amplitude is increasing with the increase in ω.

5.3. *The impact of the thermal relaxation time*

In the present case, we consider an alternate estimation of thermal relaxation time τ_0 when temperature pulse ω and the modified couple stress parameter ℓ remain constants ($\omega = 0.2$, $\ell = 0.2$). The graphs in Figs. 16-22 speak to the curves anticipated by two unique theories of thermoelasticity got as exceptional instances of the current LS model. The calculations are done for different estimations of the parameter τ_0 to get the coupled stress theory ($\ell = 0.2$) based upon the classical coupled thermoelasticity (CTE) ($\tau_0 = 0$) theory and the simple Lord-Shulman (LS) theory ($\tau_0 > 0$). It is known that the parameter τ_0 greatly affects the distributions of field factors.

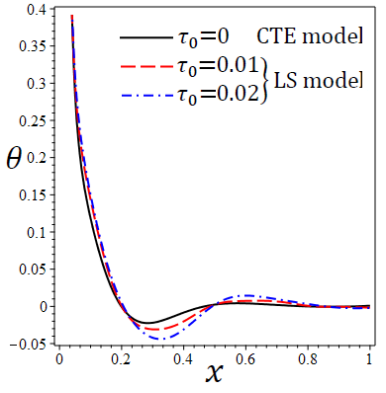

Fig. 16: Comparison between the coupled stress CTE and LS theories on the temperature θ versus axial direction ($\ell = 0.2$, $\omega = 0.2$).

Figure 16 demonstrates the temperature change θ of the microbeam through the x-axis for different values of the relaxation time τ_0 when the parameters ω and ℓ are fixed. It is well known that the value of τ_0 has a sensitive effect on the temperature values. Also, the temperature decreases monotonically in microbeams in direction of wave propagation. The wavelength of the temperature wave is constant while the amplitude increases as τ_0 increases.

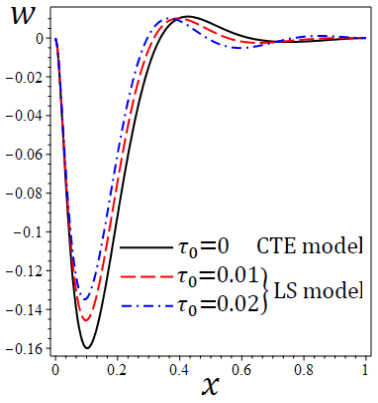

Fig. 17: Comparison between the coupled stress CTE and LS theories on the deflection w versus axial direction ($\ell = 0.2$, $\omega = 0.2$).

Figure 17 displays the variations of deflection w of the microbeam for different values of the relaxation time τ_0. Also, the deflection waves have the same wavelength while the amplitude of the deflection wave increases as τ_0 decreases. The maximum amplitudes occur for the CTE model.

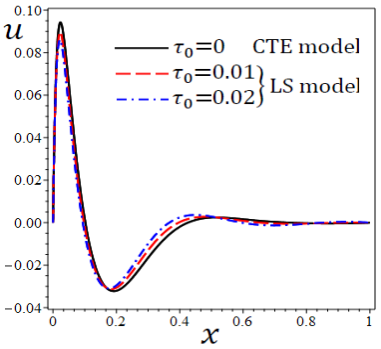

Fig. 18: Comparison between the coupled stress CTE and LS theories on the axial displacement u versus axial direction ($\ell = 0.2$, $\omega = 0.2$).

Figure 18 presents the distribution of axial displacement u of microbeam for different values of the relaxation time τ_0. The parameter τ_0 has a little effect on the distribution of displacement u. The amplitude of the displacement wave is fading away with the increase in x-axis.

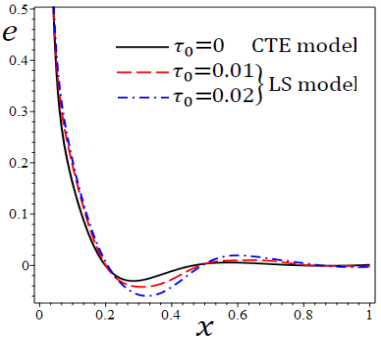

Fig. 19: Comparison between the coupled stress CTE and LS theories on dilatation e versus axial direction ($\ell = 0.2$, $\omega = 0.2$).

Figure 19 presents the distribution of dilatation e of microbeam for different values of the relaxation time τ_0. The parameter τ_0 affects the distribution of dilatation e. The amplitude of the dilatation wave is fading away with the

increase in x-axis. The wavelength of the displacement wave is constant while the amplitude is decreasing as ω increases.

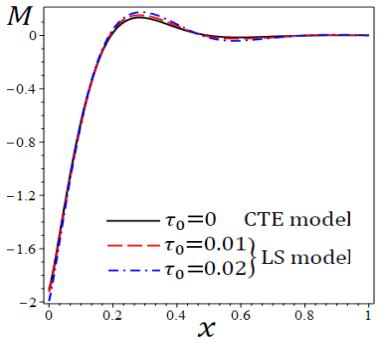

Fig. 20: Comparison between the coupled stress CTE and LS theories on the moment M versus axial direction ($\ell = 0.2, \omega = 0.2$).

Figure 20 illustrates the variety of bending moment M through axial distance x for different values of the relaxation time τ_0. It is noticed that τ_0 is slowly affected the bending moment distribution. The moment M is no longer increasing as x increases and has its maximum value when $\tau_0 = 0.02$.

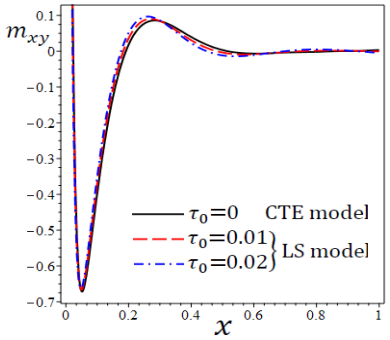

Fig. 21: Comparison between the coupled stress CTE and LS theories on the couple stress m_{xy} versus axial direction ($\ell = 0.2, \omega = 0.2$).

Figure 21 presents the distribution of couple stress m_{xy} of microbeam for different values of the relaxation time τ_0. It tends to be seen that parameter τ_0 slowly affects the distribution of m_{xy}. The amplitude of the couple stress wave is fading away with the increase in x-axis. The wavelength of the stress wave is constant while the amplitude may be increasing with the increase in τ_0.

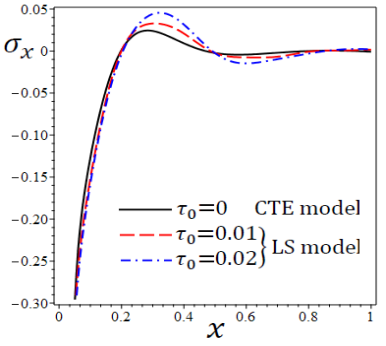

Fig. 22: Comparison between the coupled stress CTE and LS theories on the axial stress σ_x versus axial direction ($\ell = 0.2, \omega = 0.2$).

Figure 22 presents the distribution of axial stress σ_x of microbeam for different values of the relaxation time τ_0. The parameter τ_0 greatly affects the distribution of σ_x. The amplitude of the stress wave is fading away with the increase in x-axis. The wavelength of the stress wave is constant while the amplitude is increasing with the increase in τ_0.

6. Conclusions

In the current study, we consider the newly developed theory of thermoelasticity based on a single delay term to be introduced into the thermal conduction equation. The system of the governing equations of the introduced model has been derived based on Hamilton's principle for Euler–Bernoulli microbeam, modified couple stress theory, and generalized thermoelasticity theory. We are attempting to study a small-sized microbeam subject to varying temperature pulse heating. Solutions of the physical fields of the microbeam are obtained by applying the Laplace technique. Numerical technique has also been used to obtain solutions to different variables of microbeam in the physical space.

Both the analytical and numerical studies of ruling equations show a significant influence on the temperature pulse and the material length scale parameters. Also, the numerical results reveal that, in the presence of couple stress, the profiles of the studied fields of CTE theory are smaller compared to simple LS theory, and the opposite behavior is detected in lack of couple stress.

This investigation is necessary for microscale issues because in these cases material parameters reply upon temperature. Additionally, outcomes got can be significant for mechanical specialists in planning small-sized resonators for MEMS applications. Finally, the current model may be used as a piece of microelectromechanical applications, for instance, move switches, mass stream sensors, repeat channels, and resonators as well as accelerometers.

Acknowledgments

This project was funded by the Deanship of Scientific Research (DSR) at King Abdulaziz University, Jeddah, under grant no. (G: 527-130-1441). The authors, therefore, acknowledge with thanks DSR for technical and financial support.

Conflict of interest statement

The authors declare that they have no conflict of interest.

References

[1] A. M. Zenkour, A. E. Abouelregal, Effect of harmonically varying heat on FG nanobeams in the context of a nonlocal two-temperature thermoelasticity theory, *European Journal of Computational Mechanics*, Vol. 23, No. 1-2, pp. 1-14, 2014.

[2] E. Carrera, A. Abouelregal, I. Abbas, A. Zenkour, Vibrational analysis for an axially moving microbeam with two temperatures, *Journal of Thermal Stresses*, Vol. 38, No. 6, pp. 569-590, 2015.

[3] A. E. Abouelregal, A. M. Zenkour, Thermoelastic problem of an axially moving microbeam subjected to an external transverse excitation, *Journal of Theoretical and Applied Mechanics*, Vol. 53, No. 1, pp. 167-178, 2015.

[4] A. Abouelregal, A. Zenkour, Effect of phase lags on thermoelastic functionally graded microbeams subjected to ramp-type heating, *Iranian Journal of Science and Technology. Transactions of Mechanical Engineering*, Vol. 38, No. M2, pp. 321, 2014.

[5] W. Duan, C. M. Wang, Exact solutions for axisymmetric bending of micro/nanoscale circular plates based on nonlocal plate theory, *Nanotechnology*, Vol. 18, No. 38, pp. 385704, 2007.

[6] Q. Wang, K. Liew, Application of nonlocal continuum mechanics to static analysis of micro-and nano-structures, *Physics Letters A*, Vol. 363, No. 3, pp. 236-242, 2007.

[7] G. Rezazadeh, F. Khatami, A. Tahmasebi, Investigation of the torsion and bending effects on static stability of electrostatic torsional micromirrors, *Microsystem Technologies*, Vol. 13, No. 7, pp. 715-722, 2007.

[8] J.-Y. Chen, Y.-C. Hsu, S.-S. Lee, T. Mukherjee, G. K. Fedder, Modeling and simulation of a condenser microphone, *Sensors and Actuators A: Physical*, Vol. 145, pp. 224-230, 2008.

[9] A. C. Chong, D. C. Lam, Strain gradient plasticity effect in indentation hardness of polymers, *Journal of Materials Research*, Vol. 14, No. 10, pp. 4103-4110, 1999.

[10] A. W. McFarland, J. S. Colton, Role of material microstructure in plate stiffness with relevance to microcantilever sensors, *Journal of Micromechanics and Microengineering*, Vol. 15, No. 5, pp. 1060, 2005.

[11] J. Reddy, Microstructure-dependent couple stress theories of functionally graded beams, *Journal of the Mechanics and Physics of Solids*, Vol. 59, No. 11, pp. 2382-2399, 2011.

[12] F. Yang, A. Chong, D. C. C. Lam, P. Tong, Couple stress based strain gradient theory for elasticity, *International journal of solids and structures*, Vol. 39, No. 10, pp. 2731-2743, 2002.

[13] M. Malikan, Buckling analysis of a micro composite plate with nano coating based on the modified couple stress theory, *Journal of Applied and Computational Mechanics*, Vol. 4, No. 1, pp. 1-15, 2018.

[14] M. Malikan, Electro-thermal buckling of elastically supported double-layered piezoelectric nanoplates affected by an external electric voltage, *Multidiscipline Modeling in Materials and Structures*, 2019.

[15] B. Akgöz, Ö. Civalek, A size-dependent shear deformation beam model based on the strain gradient elasticity theory, *International Journal of Engineering Science*, Vol. 70, pp. 1-14, 2013.

[16] B. Akgöz, Ö. Civalek, Strain gradient elasticity and modified couple stress models for buckling analysis of axially loaded micro-scaled beams, *International Journal of Engineering Science*, Vol. 49, No. 11, pp. 1268-1280, 2011.

[17] M. Malikan, V. B. Nguyen, R. Dimitri, F. Tornabene, Dynamic modeling of non-cylindrical curved viscoelastic single-walled carbon nanotubes based on the second gradient theory, *Materials Research Express*, Vol. 6, No. 7, pp. 075041, 2019.

[18] M. Malikan, R. Dimitri, F. Tornabene, Transient response of oscillated carbon nanotubes with an internal and external damping, *Composites Part B: Engineering*, Vol. 158, pp. 198-205, 2019.

[19] G.-L. She, F.-G. Yuan, Y.-R. Ren, H.-B. Liu, W.-S. Xiao, Nonlinear bending and vibration analysis of functionally graded porous tubes via a nonlocal strain gradient theory, *Composite Structures*, Vol. 203, pp. 614-623, 2018.

[20] A. C. Eringen, D. Edelen, On nonlocal elasticity, *International journal of engineering science*, Vol. 10, No. 3, pp. 233-248, 1972.

[21] A. C. Eringen, On differential equations of nonlocal elasticity and solutions of screw dislocation and surface waves, *Journal of applied physics*, Vol. 54, No. 9, pp. 4703-4710, 1983.

[22] M. Malikan, V. B. Nguyen, A novel one-variable first-order shear deformation theory for biaxial buckling of a size-dependent plate based on Eringen's nonlocal differential law, *World Journal of Engineering*, 2018.

[23] M. Malikan, On the buckling response of axially pressurized nanotubes based on a novel nonlocal beam theory, *Journal of Applied and Computational Mechanics*, Vol. 5, No. 1, pp. 103-112, 2019.

[24] R. Ansari, J. Torabi, Nonlocal vibration analysis of circular double-layered graphene sheets resting on an elastic foundation subjected to thermal loading, *Acta Mechanica Sinica*, Vol. 32, No. 5, pp. 841-853, 2016.

[25] M. Ahmad Pour, M. Golmakani, M. Malikan, Thermal buckling analysis of circular bilayer graphene sheets resting on an elastic matrix based on nonlocal continuum mechanics, *Journal of Applied and Computational Mechanics*, Vol. 7, No. 4, pp. 1862-1877, 2021.

[26] R. Mindlin, H. Tiersten, *Effects of couple-stresses in linear elasticity*, Columbia Univ New York, pp. 1962.

[27] R. Toupin, Elastic materials with couple-stresses, *Archive for rational mechanics and analysis*, Vol. 11, No. 1, pp. 385-414, 1962.

[28] K. Rajneesh, Response of thermoelastic beam due to thermal source in modified couple stress theory, *CMST*, Vol. 22, No. 2, pp. 95-101, 2016.

[29] S. Park, X. Gao, Bernoulli–Euler beam model based on a modified couple stress theory, *Journal of Micromechanics and Microengineering*, Vol. 16, No. 11, pp. 2355, 2006.

[30] A. Abouelregal, Response of thermoelastic microbeams to a periodic external transverse excitation based on MCS theory, *Microsystem Technologies*, Vol. 24, No. 4, pp. 1925-1933, 2018.

[31] A. Zenkour, Refined two-temperature multi-phase-lags theory for thermomechanical response of microbeams using the modified couple stress analysis, *Acta Mechanica*, Vol. 229, No. 9, pp. 3671-3692, 2018.

[32] M. M. Benhamed, A. Abouelregal, Influence of temperature pulse on a nickel microbeams under couple stress theory, *Journal of Applied and Computational Mechanics*, Vol. 6, No. 4, pp. 777-787, 2020.

[33] A. M. Zenkour, Modified couple stress theory for micro-machined beam resonators with linearly varying thickness and various boundary conditions, *Archive of Mechanical Engineering*, Vol. 65, No. 1, 2018.

[34] M. Shishesaz, M. Hosseini, K. Naderan Tahan, A. Hadi, Analysis of functionally graded nanodisks under thermoelastic loading based on the strain gradient theory, *Acta Mechanica*, Vol. 228, No. 12, pp. 4141-4168, 2017.

[35] A. Hadi, M. Z. Nejad, M. Hosseini, Vibrations of three-dimensionally graded nanobeams, *International Journal of Engineering Science*, Vol. 128, pp. 12-23, 2018.

[36] A. Hadi, M. Z. Nejad, A. Rastgoo, M. Hosseini, Buckling analysis of FGM Euler-Bernoulli nano-beams with 3D-varying properties based on consistent couple-stress theory, *Steel and Composite Structures, An International Journal*, Vol. 26, No. 6, pp. 663-672, 2018.

[37] M. Hosseini, A. Hadi, A. Malekshahi, M. Shishesaz, A review of size-dependent elasticity for nanostructures, *Journal of Computational Applied Mechanics*, Vol. 49, No. 1, pp. 197-211, 2018.

[38] M. M. Khoram, M. Hosseini, A. Hadi, M. Shishehsaz, Bending analysis of bidirectional FGM Timoshenko nanobeam subjected to mechanical and magnetic forces and resting on Winkler–Pasternak foundation, *International Journal of Applied Mechanics*, Vol. 12, No. 08, pp. 2050093, 2020.

[39] H. W. Lord, Y. Shulman, A generalized dynamical theory of thermoelasticity, *Journal of the Mechanics and Physics of Solids*, Vol. 15, No. 5, pp. 299-309, 1967.

[40] A. R. Hadjesfandiari, G. F. Dargush, Couple stress theory for solids, *International Journal of Solids and Structures*, Vol. 48, No. 18, pp. 2496-2510, 2011.

[41] G. Hoing, A method for the numerical inversion of the Laplace transform, *J. Comp. Appl. Math.*, Vol. 10, pp. 113-132, 1984.

[42] D. Y. Tzou, Experimental support for the lagging behavior in heat propagation, *Journal of thermophysics and heat transfer*, Vol. 9, No. 4, pp. 686-693, 1995.